ELSEVIER

Journal of Materials Processing Technology 133 (2003) 257–265

Journal of Materials Processing Technology

www.elsevier.com/locate/jmatprotec

Effect of chill thickness and superheat on casting/chill interfacial heat transfer during solidification of commercially pure aluminium

M.A. Gafur[a], M. Nasrul Haque[b], K. Narayan Prabhu[c,*]

[a]PP&PDC, Bangladesh Council of Scientific and Industrial Research, Dhaka 1205, Bangladesh
[b]Department of Materials and Metallurgical Engineering, Bangladesh University of Engineering and Technology, Dhaka 1000, Bangladesh
[c]Department of Metallurgical and Materials Engineering, National Institute of Technology, Srinivasnagar, Surathkal 575025, India

Received 22 February 2001; received in revised form 10 January 2002; accepted 28 June 2002

Abstract

Heat transfer at the metal/chill interface during solidification of commercially pure aluminium square bar castings with cast iron chill at one end was investigated. Experiments were carried out for different chill thicknesses and superheats. The inner surface temperature of the chill initially was found to increase at a faster rate for higher superheats. The effect of chill thickness on the inner surface temperature of the chill was observed only after the heat from the solidifying casting had sufficient time to diffuse to the interior of the chill material.

Inverse analysis of the non-linear one-dimensional Fourier heat conduction equation indicated the occurrence of peak heat flux at the end of filling of the mould. The effect of superheat on heat flux was minimal after filling. However, the effect of chill thickness had a significant effect on the heat flux after the occurrence of peak heat flux. Higher heat flux transients were estimated for castings poured at higher superheats. The corresponding heat transfer coefficients were also estimated and reported. The heat flux model presented in this work can be used for determination of casting/chill interfacial heat flux as a function of chill thickness and superheat. These heat flux transients could be used as boundary conditions during numerical simulation of solidification of the casting.

Keywords: Casting/chill interface; Solidification; Inverse analysis; Chill thickness; Superheat

1. Introduction

In recent years, numerical modelling of casting solidification is receiving increasing attention because of its enormous potential in increasing productivity of the metal casting industry by reducing the time associated with the traditional experimental based design of castings [1]. Further, the computer simulation of solidification of castings offers a basis for predicting the solidification patterns and casting defects with greater accuracy. However, the success of any commercially available solidification simulation package depends to a large extent on the use of accurate thermo-physical data and boundary conditions by the solidification modeller.

The use of chills during freezing of aluminium alloys plays a major role in promoting the directional solidification. One of the important factors that affects heat transfer from the solidifying casting to chills is the resistance offered by the casting/chill interface [1,2]. The interface becomes significant when the metal and the chill have reasonable good rates of thermal conductance [3]. Many researchers [4–6] have contributed to the understanding of the heat transfer at the metal/mould interface which can be characterized either by a interfacial heat flux (q) or interfacial heat transfer coefficient (h). The interfacial heat transfer coefficient has been shown to be a function of time, mould wall thickness, mould surface roughness, mould and casting material and die coats [9,10]. A common observation was the initial rise in the heat flux transients followed by gradual decrease with the progress of solidification. Sully [11] attributed the initial increase in the heat transfer coefficient due to increase in the metallostatic pressure during filling of the mould with the liquid metal.

A generalized temperature boundary condition coupling strategy for the modeling of conventional casting processes was implemented by Trovant and Argyropoulos [12,13]. The formation of an air gap at the metal–mold interface was isolated as the most significant variable and a semi-empirical inverse equation was proposed by them to quantify the heat transfer coefficient–air gap relation across a varying range of moulds with varying thermo-physical properties. The experimental findings were then incorporated into a numerical

* Corresponding author.

0924-0136/02/$ – see front matter
PII: S0924-0136(02)00459-4

Nomenclature

c	distance between interface and position C
ChT	chill thickness
CR	correlation coefficient
d	distance between interface and position D
h	heat transfer coefficient
H	enthalpy
I	upper limit in Eqs. (2) and (3)
k	thermal conductivity
m	small integer
q	heat flux
q_{max}	maximum heat flux
Q	total heat flow
r	number of future temperature + 1
SH	superheat
t	time
T	temperature
T_C	temperature at location C
T_{CS}	temperature at casting surface
T_{chS}	temperature at the chill inner surface
T_D	temperature at location D
x	distance
Y	measured temperature

Greak letters

ρ	density
ϕ	sensitivity coefficient

model to determine the temperature boundary conditions on a real-time basis and further to improve the accuracy of casting simulations.

In the present work, the effect of superheat and chill thickness on the interfacial heat transfer during solidification of commercially pure aluminium has been investigated by estimating the heat flux transients and heat transfer coefficients at the casting/chill interface.

2. Experimental

Commercially pure aluminium (Al, 99.5%; Fe, 0.25%, Cu, 0.15%, balance others) was melted in a gas fired pit furnace. The liquid metal was degassed using hexachloroethane tablets before pouring into the mould. For fluxing, ammonium chloride was used.

Fig. 1 shows the sketch of the 3-bar sand mould used in experimentation. K-type thermocouples of diameter 0.5 mm were inserted into the chill and the casting. All of the thermocouples were connected to a Keithly 740 system scanning thermometer interfaced with a PC for acquiring the temperature data. Fig. 2 shows the different modules of the data acquisition hardware. Table 1 gives the chill dimensions and the thermocouple positions in the casting and the chill. The superheats used during casting were in the range 45–140 °C. The sand mould and the chills were dried completely before pouring the liquid metal into the mould.

2.1. Estimation of heat flux

The one-dimensional heat conduction equation

$$\frac{\partial}{\partial x}\left(k\frac{\partial T}{\partial x}\right) = \rho\frac{\partial H}{\partial t} \tag{1}$$

was solved inversely using Beck's non-linear estimation technique and was subjected to the following initial and boundary conditions.

$$T(d,t) = T_D(t), \qquad T(x,0) = T_i(x), \qquad T(c,t) = T_C(t)$$

The other boundary condition $q(0,t)$ was estimated by minimizing

$$F(q) = \sum_{i=1}^{I=mr}(T_{\eta+i} - Y_{\eta+i})^2 \tag{2}$$

The problem is to find the value of q, which minimises the sum of the square deviation of the experimental temperature from the estimated temperatures. The terms, $Y_{\eta+i}$ and $T_{\eta+i}$ are the measured and calculated temperatures at location C at time t.

The non-linear estimation procedure determines the value of q which minimises $F(q)$ given in Eq. (2)

$$\sum_{i=1}^{I=mr}(T_{\eta+i} - Y_{\eta+i})\frac{\partial T_{\eta+i}}{\partial q} = 0 \tag{3}$$

$\partial T_{\eta+i}/\partial q$ is the sensitivity coefficient, $\phi_{\eta+i}$. The above equation can be solved by a Taylor series expansion. For the lth iteration, the Taylor series approximation is given as

$$T^l_{\eta+i} \approx T^{l-1}_{\eta+i} + \frac{\partial T^{l-1}_{\eta+i}}{\partial q^l_{M+1}}(q^l_{M+1} - q^{l-1}_{M+1}) \tag{4}$$

The sensitivity coefficient was calculated using

$$\phi^{l-1}_i \equiv \frac{\partial T^{l-1}_{\eta+i}}{\partial q^l_{M+1}} \approx \frac{T_{\eta+i}(q^{l-1}_{M+1}(1+\varepsilon)) - T_{\eta+i}(q^{l-1}_{M+1})}{\varepsilon q^{l-1}_{M+1}} \tag{5}$$

The Fourier heat conduction given by (1) was approximated by explicit finite difference method as follows:

$$k\left(\frac{T_{i+1} - 2T_i + T_{i-1}}{\Delta x^2}\right) + B\left(\frac{T_{i+1} - T_{i-1}}{2\Delta x}\right)^2 = \rho\frac{H^{j+1} - H^j}{\Delta t},$$

$$k\left(\frac{T_{i+1} - 2T_i + T_{i-1}}{\Delta x^2}\right) + B\left(\frac{T_{i+1} - T_{i-1}}{2\Delta x}\right)^2 = \frac{H^{j+1} - H^j}{Z},$$

$$\text{where } B = \frac{\partial k}{\partial T}, Z = \frac{\Delta t}{\rho},$$

$$H^{j+1} = H^j + Z\left[\frac{k}{\Delta x^2}(T_{i+1} - 2T_i + T_{i-1}) + B\left(\frac{T_{i+1} - T_{i-1}}{2\Delta x}\right)^2\right] \tag{6}$$

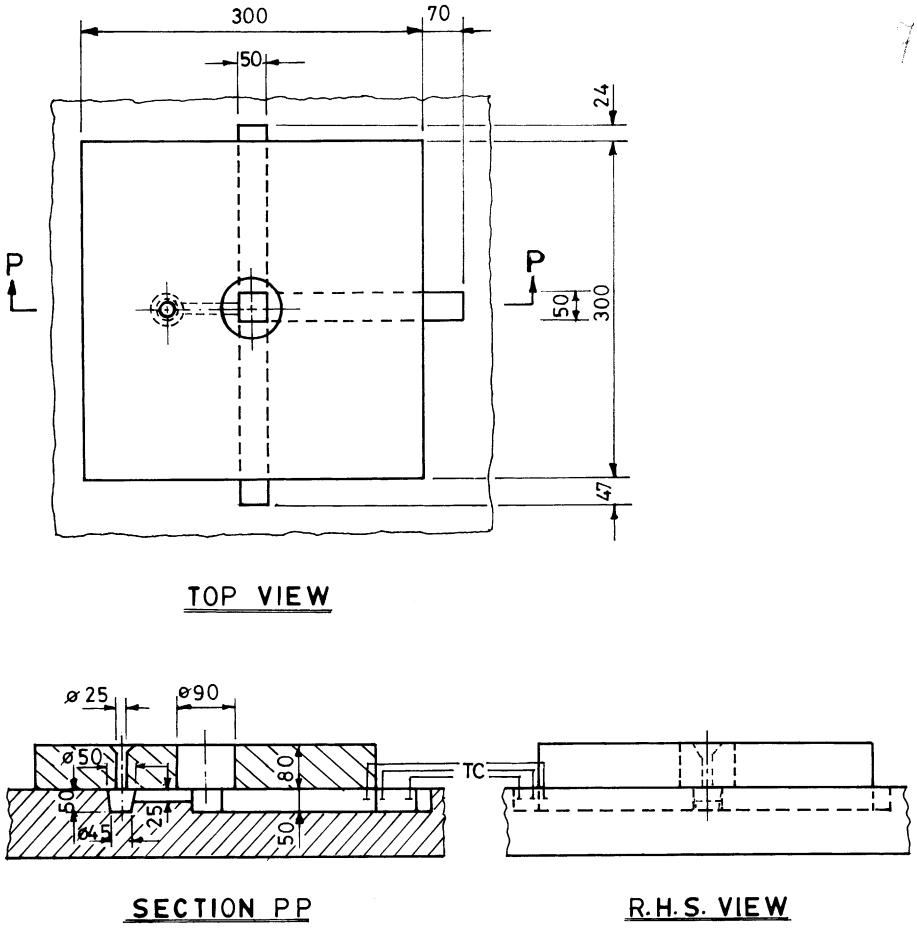

Fig. 1. A 3-bar casting with end chills.

Fig. 3 shows a typical thermal history at positions C and D. The temperature data obtained from the thermocouple near the interface was used as the known temperature history $T_C(t)$ for estimating the heat flux. The temperature data from the thermocouple near the outer surface of the chill was used as one of the boundary conditions, $T_D(t)$.

The unknown boundary condition $q(0,t)$ and the temperature $T_C(t)$ were vectorized with $\Delta\theta$ and Δt as 1 s.

Now from Eqs. (4) and (5) the correction can be obtained as

$$\nabla q_{M+1}^{l} = \frac{\sum_{i=1}^{I=mr}(Y_{\eta+i} - T_{\eta+i})\phi_i^{l-1}}{\sum_{i=1}^{I}(\phi_i^{l-1})^2} \tag{7}$$

So, the new value of q is

$$q_{M+1}^{l} = q_{M+1}^{l-1} + \nabla q_{M+1}^{l} \tag{8}$$

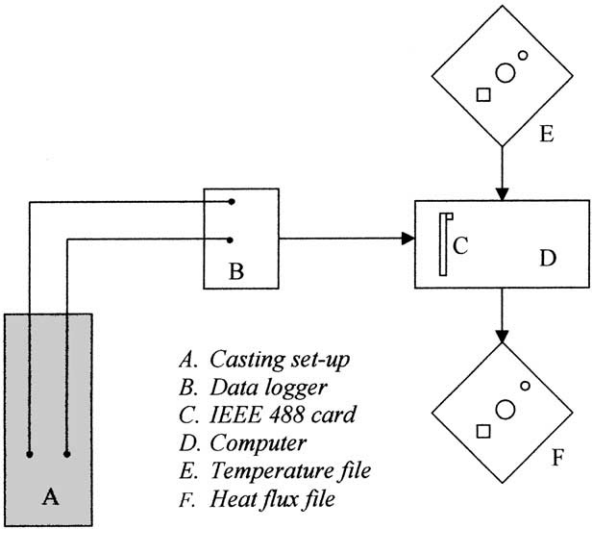

Fig. 2. Different modules of the data acquisition setup.

Table 1
Chill dimensions and thermocouple locations in the casting and the chill

Chill dimensions (mm)	Thermocouple position from the interface (mm)		
	Casting	Chill	
	Thermocouple 1 (B)	Thermocouple 2 (C)	Thermocouple 3 (D)
50 × 50 × 24	4	4	20
50 × 50 × 47	4	4	43
50 × 50 × 70	4	4	66

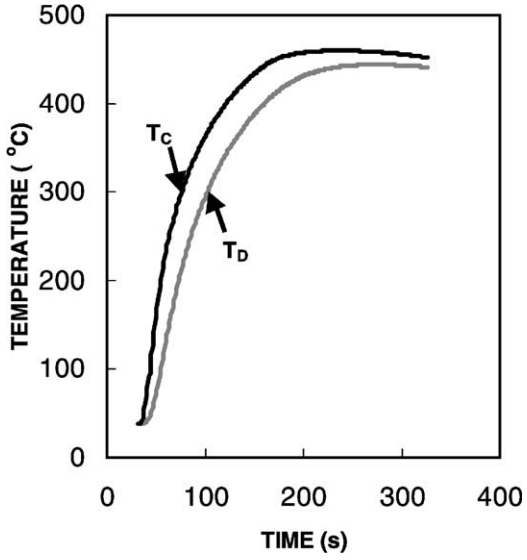

Fig. 3. Measured temperatures at locations C and D for 24 mm chill.

The procedure was repeated with q^l in place of q^{l-1} until

$$\frac{\nabla q}{q} < 0.005 \tag{9}$$

This procedure yielded the value of interfacial heat flux (q), and the surface temperature of the chill (T_{MS}) in contact with the solidifying casting. The estimated heat flux was used as one of the boundary conditions for estimation of casting surface temperature (T_{CS}). The temperature measured at location B was used as the other boundary condition. The heat transfer coefficient was calculated using the equation

$$h = \frac{q}{T_{CS} - T_{MS}} \tag{10}$$

3. Results

Figs. 4 and 5 show the effect of superheat on the thermal history for 24 mm chill at positions C and D, respectively. The increase in superheat resulted in a higher heating rate and the peak temperature attained by the chill material.

Figs. 6 and 7 show the effect of chill thickness on temperatures T_C and T_D for a casting poured at 705 °C. The thermal history revealed that initially all temperatures near the interface increased at a similar rate but after a time of about 30 s, the rate of increase of temperature of 70 mm chill became lower than the chills of lower thickness.

Fig. 8 shows the effect of superheat on the transient interfacial heat flux of bar-shaped aluminium castings with 24 mm cast iron chill at the end. The interfacial heat flux increased rapidly with time and reached a peak value for all superheats. This was followed by a sharp decrease within a few seconds. The peak value of flux increased with the

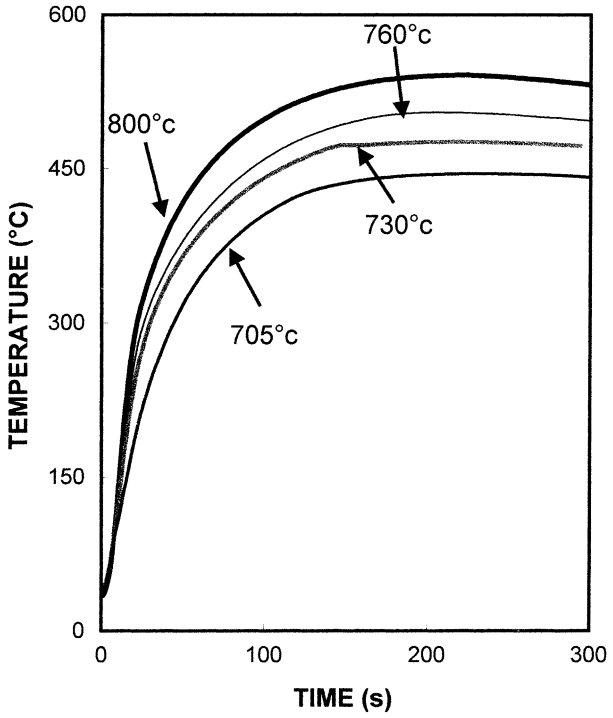

Fig. 4. Effect of superheat on temperatures measured at location C for 24 mm chill.

increase in superheat. The peak heat flux (q_{max}) was obtained at the end of filling. Peak heat fluxes of 1243 and 603 kW/m^2 were obtained for superheats of 140 and 45 °C, respectively.

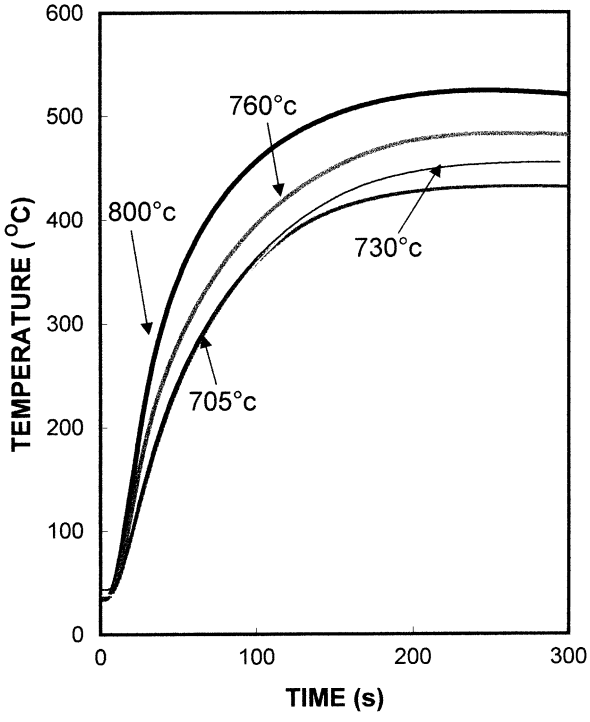

Fig. 5. Effect of superheat on temperatures measured at location D for 24 mm chill.

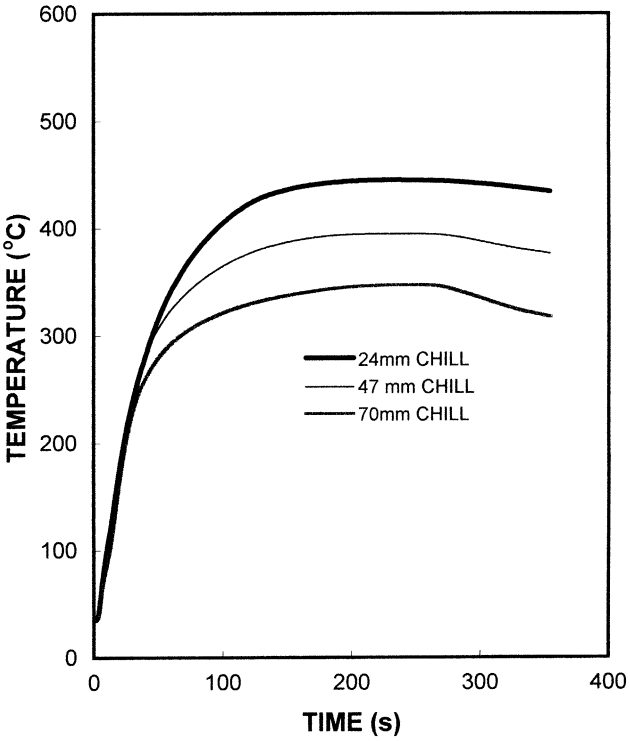

Fig. 6. Effect of chill thickness on temperatures measured at location C for a pouring temperature of 705 °C.

Fig. 9 shows the effect of chill thickness on the transient interfacial heat flux for castings poured at 800 °C. Initially, q increases from a low value to a maximum for all castings. The figures show a slight low value of q_{max} for 24 mm chill,

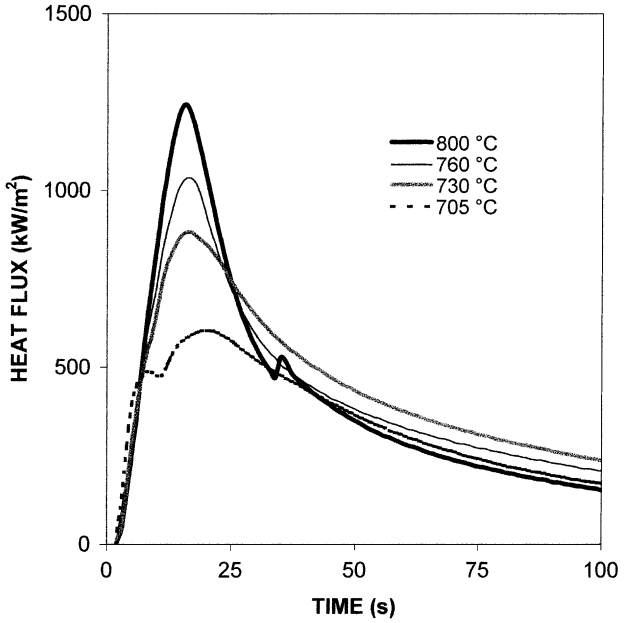

Fig. 8. Effect of superheat on heat flux transients for a 24 mm chill.

but the values are the same for larger chill thickness (47 and 70 mm). Peak heat flux values of 1243, 1287 and 1288 kW/m^2 were obtained for 24, 47 and 70 mm chills, respectively. The differences in heat flux due to the effect of chill thickness decreased with the increase in chill thickness (as can be seen from the heat flux transients for 47 and 70 mm chill).

Fig. 10 shows the effect of superheat on the total heat flow for different chill thickness for a period of 275 s after filling.

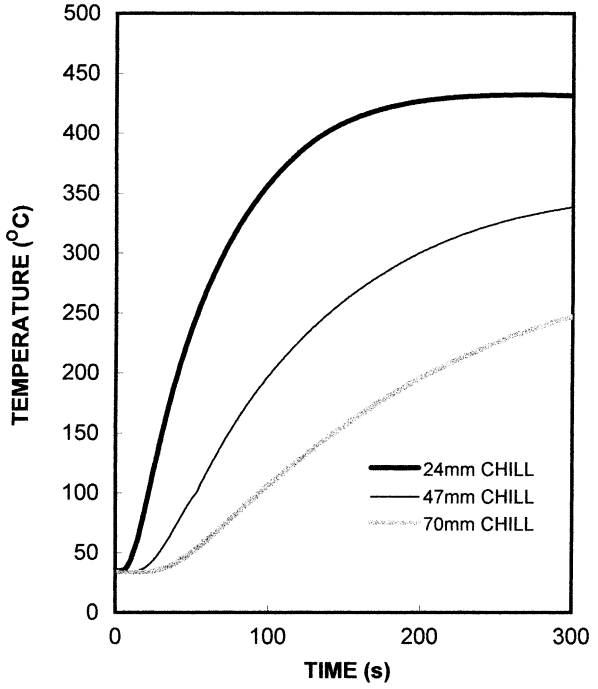

Fig. 7. Effect of chill thickness on temperatures measured at location D for a pouring temperature of 705 °C.

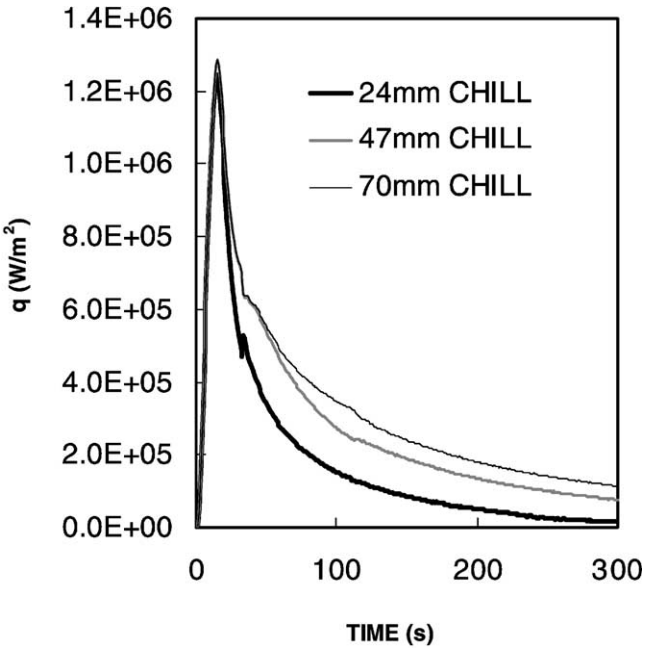

Fig. 9. Effect of chill thickness on heat flux transients for a pouring temperature of 800 °C.

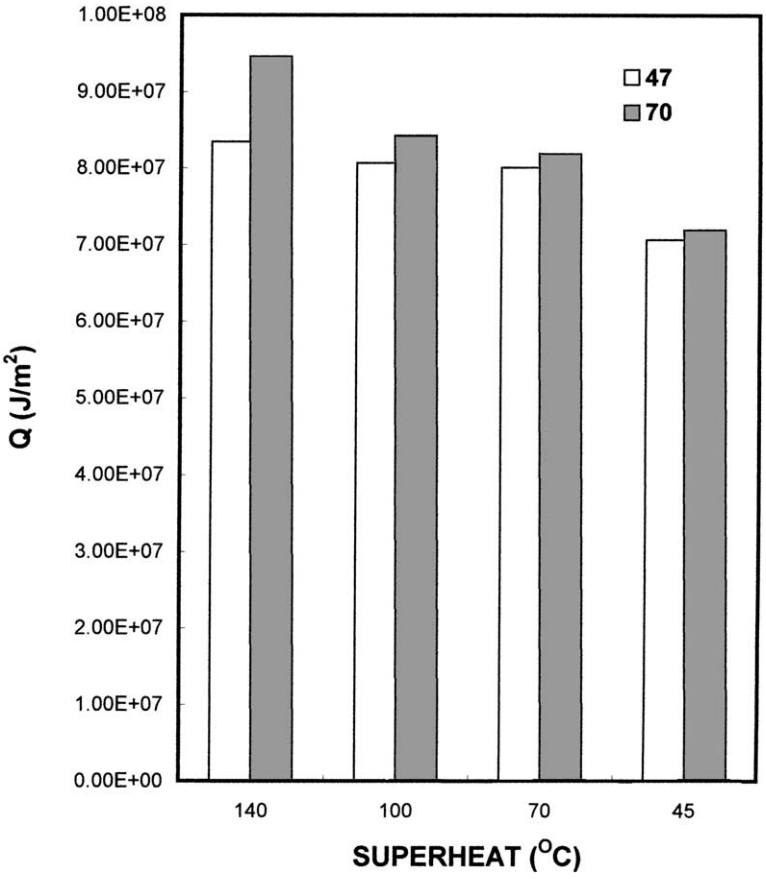

Fig. 10. Effect of superheat on heat flow for different chills.

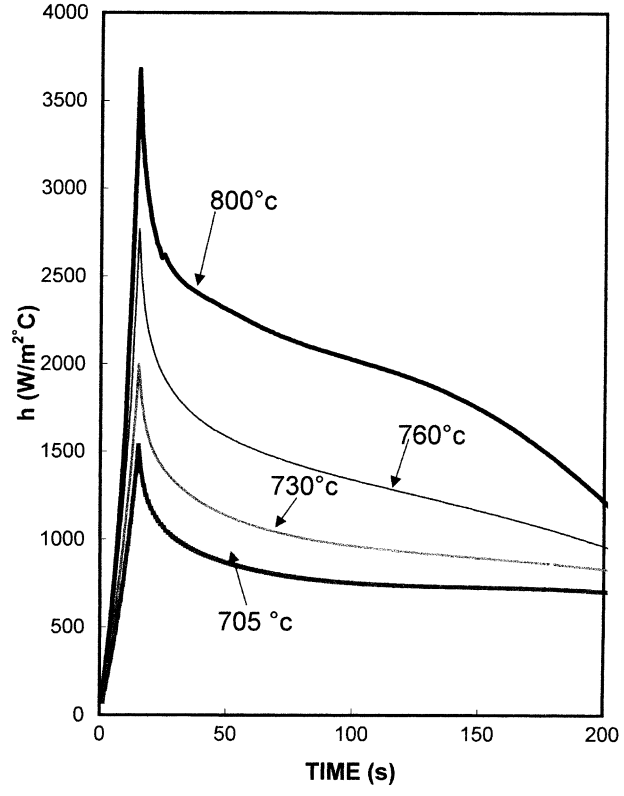

Fig. 11. Effect of superheat on heat transfer coefficient for 47 mm chill.

It shows that the total heat flow passing through the interface increases with increase in superheat and chill thickness. The figure also indicates that the difference of total heat absorption due to chill thickness decreases with the decrease in superheat and becomes negligible for a superheat of 45 °C.

Fig. 11 shows the effect of superheat on transient h for a 47 mm thick chill. The heat transfer coefficient increased from a very small value to a peak value and decreased sharply thereafter to reach a steady value. The peak heat transfer coefficients were obtained at the end of filling and were in the range 1535–3679 W/m^2 °C corresponding to superheats of 45–140 °C and the steady values obtained were in the range 900–2100 W/m^2 °C.

Fig. 12 shows the effect of chill thickness on heat transfer coefficient for a pouring temperature of 730 °C. The effect of chill thickness on heat transfer coefficient was found to be negligible.

4. Discussion

With increase in superheat, more heat flows through the chill material because of higher initial temperature difference and better casting–chill contact. This resulted in higher heating rates for the chills shown in Figs. 4 and 5. Bishop et al. [14] estimated higher mould surface temperatures for

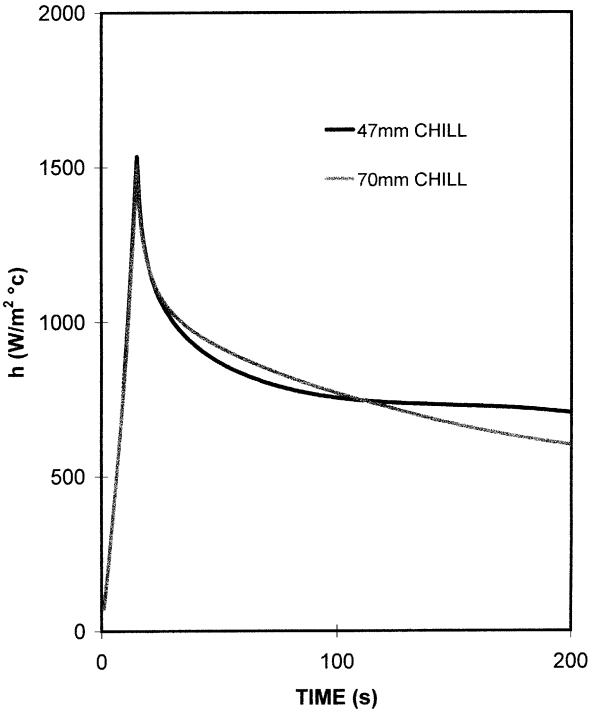

Fig. 12. Effect of chill thickness on heat transfer coefficient for a pouring temperature of 730 °C.

higher superheats of medium carbon steel poured in cast iron mould. The thermal history shown for locations C and D in Figs. 4 and 5 are similar except at the initial stage. Since the position D is far from the interface, initially there is no rise in temperature as more time is required for the heat to diffuse to location D.

Higher maximum chill temperatures were observed in lower chill thickness (Fig. 6). Initially, the rate of heating of the chill were the same for all chill thickness. When the heat diffuses to the external surface of the chill, the heat transfer from the interface is controlled by the surroundings. For the thinner chill the heat reaches the outer surface ahead of thicker one. Due to minimal transfer of heat to the surroundings, the heat is accumulated and the temperature increases more than that of the thicker one. The chill gets thermally saturated and this decreases the efficiency of chill to extract more heat from the casting. Higher the chill thickness, higher is the volumetric heat capacity and more is the heat absorbed by the thicker chill. Due to lower volumetric heat capacity, the temperature near the interface of thinner chill increases at a faster rate. Hou and Pehlke [15] found that the different thickness of chill walls resulted in different thermal capacities, causing different temperature distributions in the chills. The thinnest chill due to its lowest volumetric heat capacity resulted in continued rapid heating throughout the entire wall. The intermediate chill wall had sufficient heat capacity to maintain an approximately constant interface temperature, while the thicker one was more than sufficient so that the temperature continuously decreased after reaching the maximum.

Fig. 7 shows that the thermocouple near the external surface position D of higher chill thickness taking longer time to respond as the position D is far away from the interface for the thicker chill and hence heat takes more time to reach the location D. The heat extracted by the chill depends on the temperature gradient of the chill at the interface. When heat reaches the external surface, temperature gradient near the external surface of the chill decreases and this effect diffuses gradually towards the casting–chill interface. As a result, the temperature of the inner surface increases due to higher rate of heat accumulation. Bishop et al. [14] observed that the temperature of external surface of a 38 mm thick chill instantaneously increased, whereas, that of 105 mm chill remained at initial temperature up to about 40 s.

In the present investigation, the peak heat flux is obtained at the end of filling. As the level of liquid metal rises upward the metallostatic pressure increases continuously. When it fills the feeder at the end of filling, the metallostatic pressure is at its maximum. The contact is more intimate with increasing metallostatic pressure which resulted in the occurrence of peak heat flux at the end of filling.

To verify whether the peak is associated with the start of solidification, the pouring temperatures were varied. At the end of filling, depending on the superheat of the molten metal, the casting surface was found to be liquid ($T_{CS} = 771$ °C) as shown by the T_C curve at q_{max} in Fig. 13, or at melting point ($T_{CS} = 660$ °C) as shown in Fig. 14 or may form a solidified skin ($T_{CS} = 615$ °C) as shown in Fig. 15. The peak values of q were observed at the end of filling for each of the three conditions. Other investigators [8,16] have also observed that the heat extraction at the interface increases with increase in pressure.

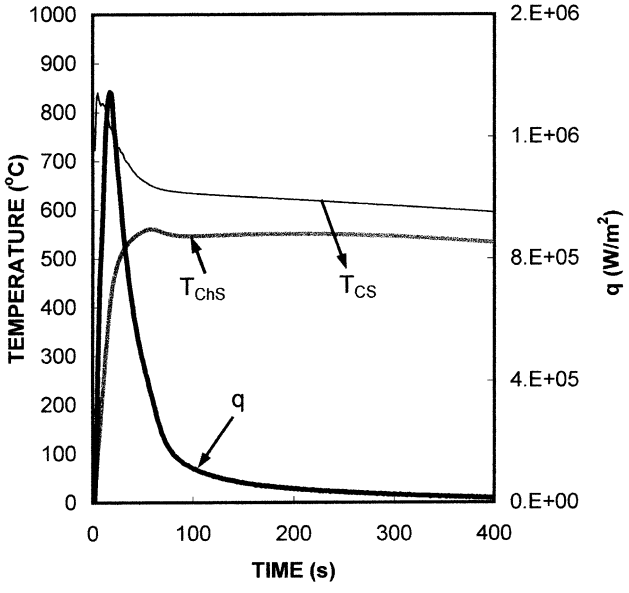

Fig. 13. Thermal history showing liquid metal at the interface at q_{max}.

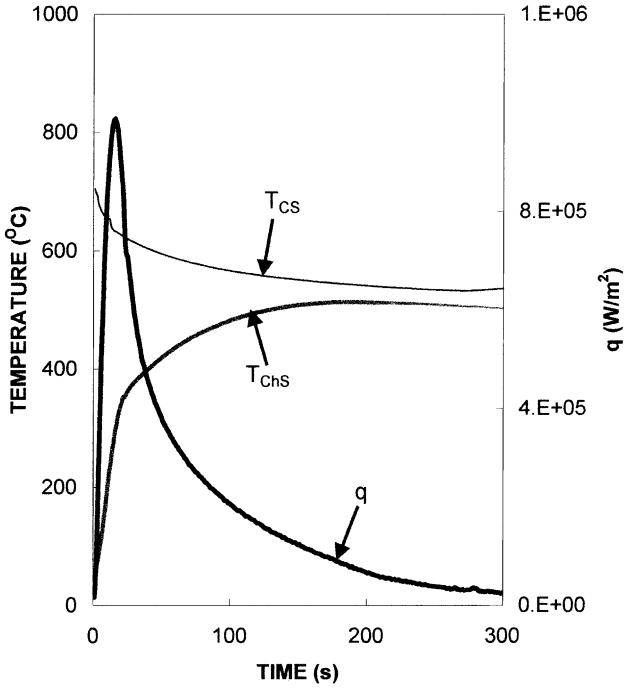

Fig. 14. Thermal history showing casting surface at the melting point at q_{max}.

At the end of filling, as the liquid level decreases due to shrinkage, the contact pressure gradually decreases. In one hand, when the melt starts to solidify, the solidified skin may have sufficient strength to initiate gap after the end of filling and it gradually increases. On the other hand, when the melt is nearly at the melting point at the end of filling the solidification proceeds with non-conforming solid–solid contact. The lowering of pressure, the non-conforming contact and the initiation of gap are all possibly responsible for the sharp fall in heat flux after the end of filling. A number of investigators [7,17] suggested that the start of solidification caused the sharp decrease in heat flux or heat transfer coefficient. The present study shows that the decrease in metallostatic pressure is also associated with the decrease in heat flux. After the sharp decrease in q, the chill surface is sufficiently heated and the difference between the T_{MS} and T_{CS} became small and decreased very slowly with time.

Fig. 8 shows that the differences in heat flux transients due to superheat decreased with time after the occurrence of peak in the heat flux. The increase in the peak heat flux with increase in superheat could be attributed to (i) the initial temperature difference $(T_{CS} - T_{MS})$ between casting and chill surfaces and (ii) better contact at the casting/chill interface owing to the lower surface tension of the liquid metal.

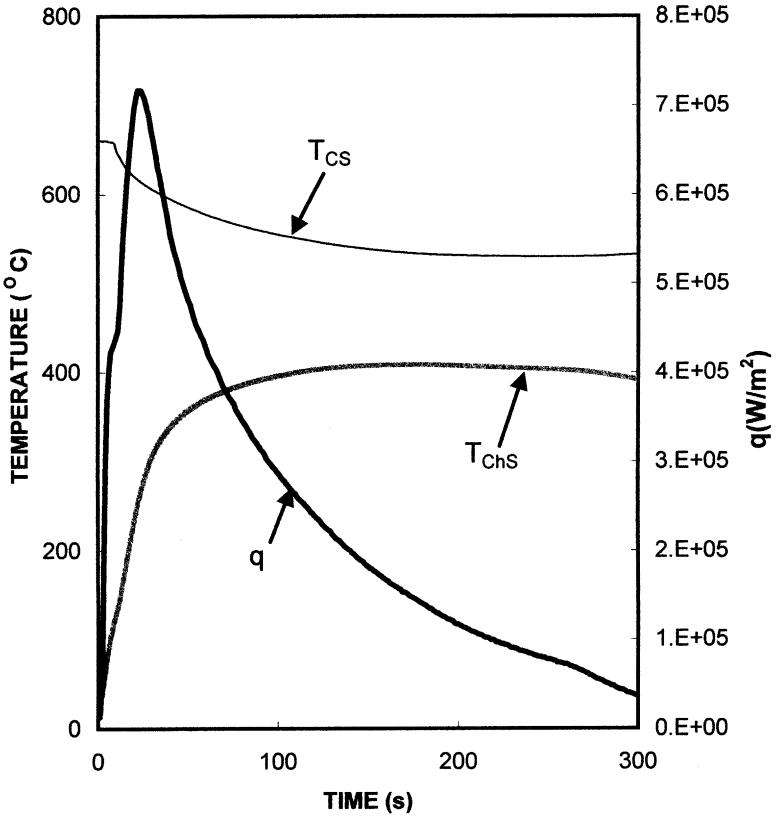

Fig. 15. Thermal history showing solidified skin at the interface at q_{max}.

Kumar and Prabhu [7] found that the peak heat flux decreased with the increase of chill thickness for aluminium alloys. In the present study, the effect of chill thickness on q_{max} is not observed for higher chill thickness (Fig. 9). For lower chill thickness the value of the peak estimated is slightly lower than that of thicker chill. The figure shows that the heat flux for the thicker chills remained high for a short period of time after the occurrence of peak flux and a slight difference in q was observed thereafter when the effect of thickness was noticed at the interface.

When the liquid is poured at high superheats, larger is the temperature difference between the casting and chill and the better is the contact and the more is the heat passing through the interface for the same span of time (275 s) as shown in Fig. 10. The effect of chill thickness on total heat flow through interface is prominent at higher superheat. For higher superheats, thinner chill is not capable of absorbing heat as much as thicker one due to its lower volumetric heat capacity.

The chill thickness had no significant effect on the heat transfer coefficient (Fig. 12). Heat transfer coefficient depends on the extent of contact between the casting and chill. This is strongly influenced by the surface condition and the wettability of the melt on the chill surface. For a given superheat, the surface condition is same for any chill thickness.

The effect of superheat on peak heat flux could be represented by a linear regression equation

$$q_{max} = 403600 + 6201 \times SH \quad (CR = 0.9898) \tag{11}$$

The initial rise in heat flux is more or less linear and could be represented as

$$\frac{q}{q_{max}} = \frac{1}{C_1} t \tag{12}$$

where C_1 is the time from the thermocouple response at C to the end of filling that is equal to the filling time—time required for thermocouple at C to respond to change in the temperature and was found to be about 15 s, t the time after the thermocouple response at location C.

The decrease in the heat flux after reaching a peak value was represented by logarithmic equation as

$$\frac{q}{q_{max}} = [1 - C_2 \ln(t - C_1)] \tag{13}$$

$$C_2 = 0.1693 - 0.4391 \times ChT + 0.0002 \times SH \times (CR = 0.9795)$$

The value of C_2 increases with increase in superheat and decreases with decrease in the chill thickness.

5. Conclusions

Based on the results and discussion, the following conclusions were drawn:

(1) Both chill thickness and superheat had a significant effect on the rate of increase of temperature of chill in contact with the solidifying casting. The increase in superheat increased the heating rate of the chill material during solidification. The effect of chill thickness was observed only after the heat diffused into the interior of the chill material and affected the external surface temperature of the chill. However, the effect of superheat was evident from the initial stages of solidification.
(2) The peak heat flux (q_{max}) was obtained at the end of filling for all experiments and was attributed to an improved contact at the casting/chill interface as a result of the increase in the metallostatic pressure at the end of filling.
(3) The peak heat flux increased with the increase in the superheat and the effect of superheat on heat flux transients was minimal after the occurrence of peak heat flux.
(4) The effect of chill thickness on the total heat flux flow was significant at higher superheats.
(5) Higher heat transfer coefficients were obtained for higher superheats. The effect of chill thickness on heat transfer coefficients was not significant.

Acknowledgements

The authors are grateful to the Dept. of Materials and Metallurgical Engineering, Bangladesh University of Engineering and Technology, Dhaka, Bangladesh, for providing excellent research facilities. One of the authors, M.A. Gafur, is indebted to BCSIR, Ministry of Science and Technology, for granting him financial support and leave to complete the work.

References

[1] H. Huang, O. Gurdogan, H.U. Akay, W.W. Fincher, AFS Trans. 103 (1995) 243.
[2] D.R. Durham, J.T. Berry, AFS Trans. 84 (1976) 101.
[3] J. Campbell, Castings, Butterworth-Hienmann Ltd., Oxford, 1991, p. 126.
[4] K. Ho, R.D. Pehlke, AFS Trans. 91 (1983) 689.
[5] K. Ho, R.D. Pehlke, AFS Trans. 92 (1984) 587.
[6] K. Ho, R.D. Pehlke, Metall. Trans. B 16 (1985) 585.
[7] T.S.P. Kumar, K.N. Prabhu, Metall. Trans. B 22 (1991) 717.
[8] M. Parets, H. Biloni, Metall. Trans. A 3 (1972) 1501.
[9] A. Morales, M.E. Glicksman, H. Bilioni, Influence of mould wall microgeometry on casting structure, in: Solidification and Casting Metals, The Metal Society, London, 1979, p. 184.
[10] A.M. Assar, Mater. Sci. Technol. 13 (1997) 702.
[11] L.J.D. Sully, AFS Trans. 84 (1976) 735.
[12] M. Trovant, S.A. Argyropoulos, Met. Mater. Trans. B 31 (2000) 75.
[13] M. Trovant, S.A. Argyropoulos, Met. Mater. Trans. B 31 (2000) 87.
[14] H.F. Bishop, F.A. Barant, W.S. Pellini, AFS Trans. 59 (1951) 435.
[15] T.X. Hou, R.D. Pehlke, AFS Trans. 88 (1988) 151.
[16] S.D. Pathak, Feeding efficiency parameters and feeding range for aluminium base alloys cast in metallic moulds, Ph.D. Thesis, Met. Dept., Indian Institute of Technology, Madras, India, 1984.
[17] V.de.L. Davies, British Foundaryman 73 (1980) 331.